Microporous and Mesoporous Materials 351 (2023) 112482

Contents lists available at ScienceDirect

Microporous and Mesoporous Materials

journal homepage: www.elsevier.com/locate/micromeso

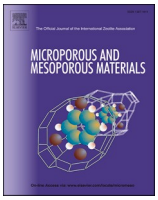

Impact of porosity and surface functionalization of hard templates on the preparation of mesoporous silica microspheres

Fabio Fait [a,b,1], Julia C. Steinbach [a,b,1], Andreas Kandelbauer [b,c], Hermann A. Mayer [a,*]

[a] Institute of Inorganic Chemistry, University of Tübingen, Auf der Morgenstelle 18, 72076, Tübingen, Germany
[b] Process Analysis and Technology (PA&T), Reutlingen Research Institute, Reutlingen University, Alteburgstrasse 150, 72762, Reutlingen, Germany
[c] Institute of Wood Technology and Renewable Materials, Department of Material Sciences and Process Engineering (MAP), University of Natural Resources and Life Sciences, Gregor-Mendel-Straße 33, 1180, Vienna, Austria

ARTICLE INFO

Keywords:
Glycidylmethacrylate (GMA)
Ethylenglycol dimethacrylate (EDMA)
Mesoporous silica microspheres (MPSM)
Hard template method
High performance liquid chromatography (HPLC)

ABSTRACT

Mesoporous silica microspheres (**MPSMs**) find broad application as separation materials in high liquid chromatography (HPLC). A promising preparation strategy uses *p*(GMA-*co*-EDMA) as hard templates to control the pore properties and a narrow size distribution of the MPMs. Here six hard templates were prepared which differ in their porosity and surface functionalization. This was achieved by altering the ratio of GMA to EDMA and by adjusting the proportion of monomer and porogen in the polymerization process. The various amounts of GMA incorporated into the polymer network of **P1**-**6** lead to different numbers of tetraethylene pentamine in the *p*(GMA-*co*-EDMA) template. This was established by a partial least squares regression (PLS-R) model, based on FTIR spectra of the templates. Deposition of silica nanoparticles (SNP) into the template under Stoeber conditions and subsequent removal of the polymer by calcination result in **MPSM1**-**6**. The size of the SNPs and their incorporation depends on the pore parameters of the template and degree of TEPA functionalization. Moreover, the incorporated SNPs construct the silica network and control the pore parameters of the **MPSMs**. Functionalization of the **MPSMs** with trimethoxy (octadecyl) silane allows their use as a stationary phase for the separation of biomolecules. The pore characteristics and the functionalization of the template determine the pore structure of the silica particles and, consequently, their separation properties.

1. Introduction

Silica based materials serve as platforms in a wide range of applications e.g. in coatings, as filler materials, in catalysis, in chemical sensors and in separation methods or medical diagnostics [1–6]. Furthermore, porous silica microspheres are widely used due to their high specific surface area, chemical stability and the possibility to vary their properties by surface functionalization [7–9]. Especially in high performance liquid chromatography (HPLC), porous silica microspheres are employed in column materials as stationary phases. With the continuous progress of HPLC and the ever-increasing demands on separation methods, further improvement of column materials is essential.

A high surface area is beneficial for separation efficiency in HPLC applications. As the relative surface area increases with decreasing particle diameter, this can be achieved by reducing the sizes of the particles. Unfortunately, this increases the backpressure which demands special and costly requirements for the HPLC equipment [10,11]. This challenge can be overcome by introducing mesopores and/or macropores into micron sized silica particles, which allow for good effective interaction of the liquid phase with the surface of the stationary phase in diffusion-controlled processes such as HPLC [12].

Currently, micron sized mesoporous silica particles are produced in industrial scale by emulsion process or spray drying [13–15]. These methods generate high yields but result in a broad particle size distribution. Processing and separation techniques such as sieving, sedimentation or air classification are necessary to obtain monodisperse particle distributions. These are costly and time-consuming.

The method presented by Stoeber et al. for the preparation of monodisperse silica particles posed a fundamental development in sol-gel chemistry. Under basic conditions the hydrolysis and condensation of alkoxysilane precursors in alcoholic media form spherical silica species. However, their size is limited to a range of 50–800 nm [16,17].

* Corresponding author.
E-mail address: hermann.mayer@uni-tuebingen.de (H.A. Mayer).
[1] Fabio Fait and Julia C. Steinbach equally contributed to this work.

https://doi.org/10.1016/j.micromeso.2023.112482
Received 3 January 2023; Received in revised form 31 January 2023; Accepted 2 February 2023
Available online 6 February 2023

Although special techniques allow to expand the particle size into the micrometer range, they remain non-porous [18–20].

The preparation of porous silica materials with discrete sizes can be achieved by different template methods [21–23]. A hard template method has been demonstrated to be suitable for the targeted synthesis of mesoporous silica microspheres (**MPSMs**) with a narrow size distribution [24–26]. Thus amino-functionalized porous organic co-polymers based on glycidyl methacrylate and ethylene glycol dimethacrylate (*p*(GMA-*co*-EDMA)) thermosets were successfully applied as hard templates in the preparation of **MPSMs** [27–29]. In the presence of these polymer templates, the hydrolysis and condensation of alkoxysilanes under Stoeber conditions generate silica nanoparticles (SNP) which accumulate in the pores of the polymer network. The SNPs aggregate in the pores and build a new silica network, which is interpenetrating the organic template. The organic polymer can be removed via calcination, leaving **MPSMs** (Scheme 1). Their morphology and pore properties are selectively controlled while maintaining a spherical shape with a narrow size distribution [24–26,30].

We reported earlier the systematic evaluation of process parameters in seeded suspension polymerization of GMA and EDMA [31]. The particle and pore properties of the polymer were controlled in targeted manner by variation of the GMA to EDMA ratio, the monomer to porogen ratio and the composition of the porogens. For *p*(GMA-*co*-EDMA) templates, higher proportions of GMA resulted in larger pores and smaller surface areas [31].

Here we demonstrate that the pore structures of the hard polymer template affect the size and pore properties of the mesoporous silica microspheres which have implications on their performance in HPLC.

2. Materials and methods

2.1. Chemicals

Polyvinyl alcohol (PVA, 87–89% hydrolyzed, mean average 88,000–97,000 g mol^{-1}), tetraethyl orthosilicate (TEOS) and trimethoxy (octadecyl) silane (ODTMS) were acquired from abcr GmbH. Ethyleneglycol dimethacrylate (EDMA) was bought from Acros Organics and ammonia (28–30% aqueous solution) was obtained from Alfa Aesar. Cyclohexanol and sodium dodecyl sulfate (SDS) were purchased from Carl Roth. Dibenzoyl peroxide (BPO), dibutyl phthalate (DBP), ethanol (EtOH), glycidyl methacrylate (GMA), hydrochloric acid, methanol (MeOH), 2-propanol, triethylamine, trifluoroacetic acid (TFA) and the protein test mixture H2899 (ribonuclease A, cytochrome C, holotransferrin and apomyoglobin) were obtained from Sigma-Aldrich. Acetonitrile (ACN, HPLC grade), tetraethylene pentamine (TEPA), and water (HPLC grade) were bought from fisher scientific. Toluene and deionized water were cleaned through a solvent purification system (SPS-800, MBraun).

2.2. Characterizations

Scanning electron microscopy (SEM) images were taken with a Hitachi SU8030 instrument and used to determine the size, dispersity, and morphology of the particles. The size and dispersity of the particles were assessed by evaluating at least 400 particles per batch. Thermogravimetric studies of the hybrid beads were performed on a Mettler Toledo TGA/DSC I. For this purpose, the samples were calcined in an alumina crucible with a heating rate of 5 K min^{-1} under synthetic air (50 mL min^{-1}). The remaining mass corresponds to the amount of silica.

Infrared (IR) spectra were acquired using a Frontier 2 FTIR (PerkinElmer) with an attenuated total reflection accessory. Each sample was measured five times in a spectral range from 4000 cm^{-1} to 500 cm^{-1} with a spectral resolution of 2 cm^{-1} and four scans. A partial least squares regression model (PLS-R) was built similar to previous work [31]. To increase model quality, another two *p*(GMA-*co*-EDMA) templates with 50:50 GMA:EDMA from previous work (central points, CPs) were added for model building. The spectra were preprocessed by smoothing with a Savitzky-Golay filter (polynomial order: 2., over eleven points) and a subsequent removal of multiplicative scattering effects using a standard normal variate transformation. The analyzed spectral range was 1750–700 cm^{-1}. The spectra of the *p*(GMA-*co*-EDMA) templates (five spectra of **P1**–**4**, two spectra from **P5** and **P6** and seven spectra from the CPs) were used as test set and were validated externally (three spectra of **P5** and **P6**, as well as three spectra of the central points from our previous work). For spectral preprocessing and the multivariate data analysis, the software Unscrambler-X (CAMO Software AS) was used. The PLS-R model was applied for the prediction of GMA content for all particles **P1**–**6** and **P1**–**6@TEPA**, to assess the change in epoxy groups after amination as indicative measure for the degree of amination.

To determine the pore size, volume, and specific surface area of the particles, N_2 adsorption-desorption measurements were performed on a BELSORP MiniX from Microtrac Retsch GmbH. The samples were preheated with a BELSORP VACII to remove possible physisorbed substances and to establish a reproducible equilibrium state. At a final vacuum of $2 \bullet 10^{-2}$ mbar, polymer samples were evacuated at 30 °C for 24 h, and silica samples were pretreated at 300 °C for 3 h, respectively. Nitrogen adsorption measurements were performed at 77 K. BELMaster 7 software was used to evaluate the isotherms. The specific surface area of the particles was determined according to the method of Brunauer, Emmett, and Teller (BET). The pore size distributions were obtained by applying the Barrett-Joyner-Halenda (BJH) method to the desorption and adsorption isotherms for the polymer templates and desorption isotherms for the silica particles. This was done taking into account that the peaks around 4 nm (Fig S3, S.I.) are the result of the tensile strength effect rather than a bimodal pore size distribution [32]. The median of the pore sizes differs hardly between adsorption and desorption isotherms (Table 1). This is the reason why the pore size distributions of the adsorption isotherms are shown in Fig. 3 for the polymer templates. The pore volume was estimated from a single point adsorption at p/p_0 of 0.95.

Analytical high performance liquid chromatography was performed on an Agilent 1100 series system (Agilent Technologies, Waldbronn, Germany) equipped with a quaternary pump with degasser, an auto

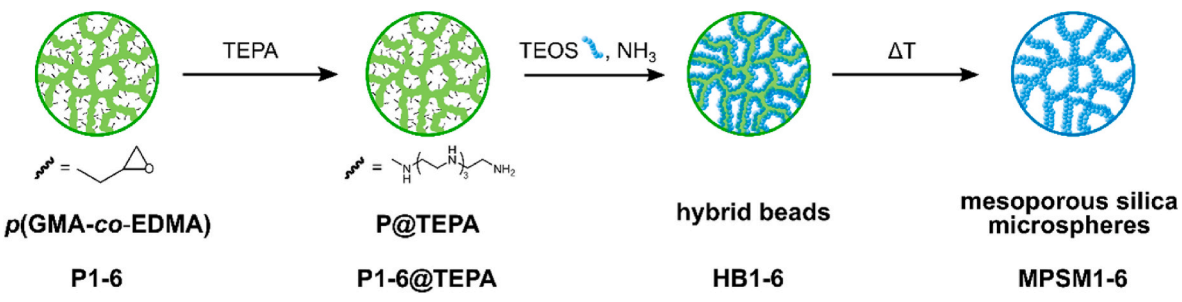

Scheme 1. Synthesis of mesoporous silica microspheres with different *p*(GMA-*co*-EDMA) polymer templates.

Table 1
Particle properties of *p*(GMA-*co*-EDMA) microspheres **P1**–**6** prepared with varying GMA/EDMA and monomer/porogen ratios.

	GMA/EDMA	monomer/porogen	particle size	dispersity	median pore size		pore volume	specific surface area
	v./v.	v./v.	[μm]	d_{90}/d_{10}	[nm][a]	[nm][b]	[$cm^3\ g^{-1}$]	[$m^2\ g^{-1}$]
P1	20/80	50/50	7.9	1.1	6.1	8.0	0.29	270
P2	40/60	50/50	7.8	1.2	12.2	12.6	0.19	123
P3	60/40	50/50	7.5	1.1	20.6	21.1	0.09	43
P4	80/20	50/50	7.3	1.2	35.5	35.4	0.03	15
P5	40/60	25/75	7.6	1.2	26.7	27.9	0.25	132
P6	40/60	75/25	7.9	1.2	15.1	8.5	0.06	31

[a] From adsorption isotherm.
[b] From desorption isotherm.

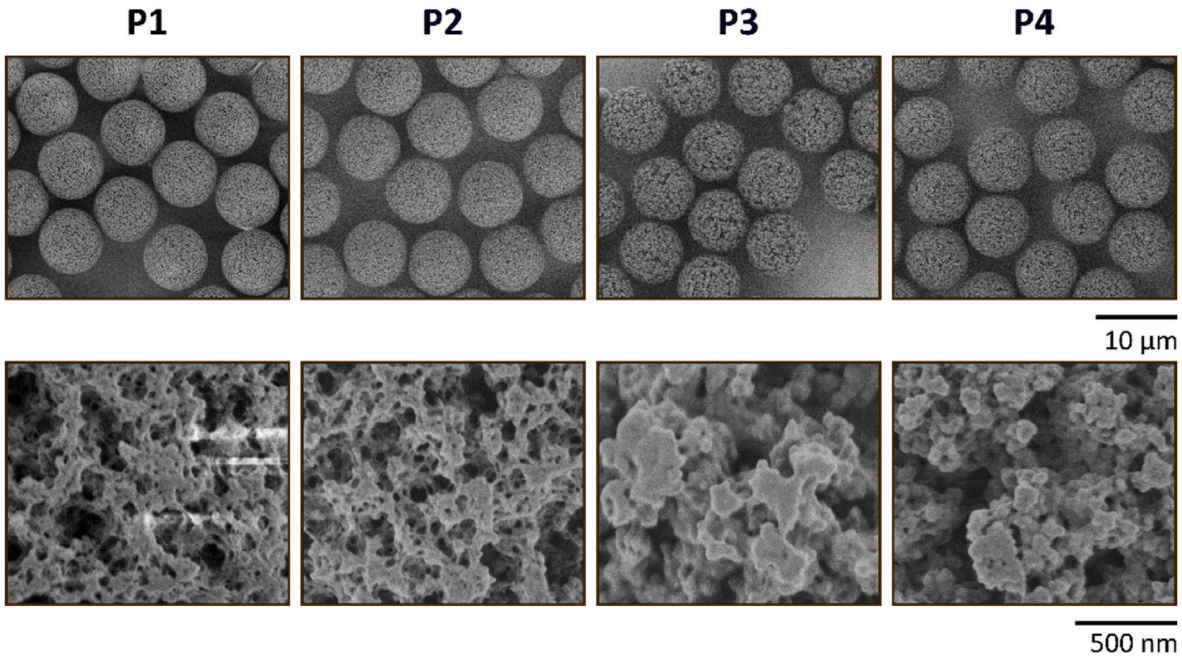

Fig. 1. SEM images of *p*(GMA-*co*-EDMA) templates **P1**–**4** with increasing GMA to EDMA ratio (from left to right). 2,000 (top row) and 50,000 (bottom row) magnification.

sampling system, column oven and a diode array detector. Instrument control, data acquisition and automated data analysis was performed by the Chem-Station software (B.04.03, Agilent Technologies, Waldbronn, Germany). A gradient elution was performed using water with 0.1% TFA (eluent A) and acetonitrile with 0.08% TFA (eluent B) with a gradient starting at 20% B to 85% B within 25 min. 5 μL of the protein mixture H2899 (1 mg mL^{-1} each protein in 90/10 A/B) were injected and detected at a wavelength of 215 nm. A commercially available column (ProSphere C18, 300 Å, 10 μm, 250 × 4.6 mm) was used as reference column. The prepared particles were packed into stainless-steel columns (250 × 4.6 mm).

2.3. Synthesis

2.3.1. Preparation of porous p(GMA-co-EDMA) particles *P1–6*

Monodisperse polystyrene (PS) microspheres with diameters of 1.9 ± 0.1 μm were prepared as reported earlier (Fig S1, S.I.) [24].

0.3 g of polystyrene particles and 5 mL of an aqueous SDS solution (0.25 wt%) were dispersed in a 250 mL flask. 2 mL of DBP were emulsified in 150 mL of an aqueous SDS solution (0.25 wt%) with a homogenizer at 4500 rpm for 15 min and then added to the polystyrene suspension. The mixture was stirred for 24 h at 200 rpm. Depending on the experiment the volume ratios of GMA and EDMA and the monomer to porogen ratios were varied according to Table 1. As porogen a mixture of toluene and cyclohexanol (73/27 v./v.) was applied. In all experiments a total volume of 30 mL of the organic phase was maintained. The monomer and porogen mixture, 0.4 g of BPO and 150 mL of an aqueous SDS solution (0.25 wt%) were emulsified with a homogenizer at 4500 rpm for 15 min. This emulsion and the activated polystyrene particles were transferred to a 500 mL three-necked flask and stirred for 24 h at 200 rpm. 150 mL of an aqueous PVA solution (2.3 wt %) was added to the reaction and Argon was passed into the reaction mixture for 30 min and then heated to 70 °C for 24 h. The particles were separated from the solution, washed three times with EtOH and three times with H_2O and dried at 65 °C for 16 h.

2.3.2. Preparation of mesoporous silica microspheres *MPSM1–6*

5 g of particles **P1**–**6** were dispersed in 200 mL of H_2O, 7.5 mL of tetraethylene pentamine were added and the solution was stirred for 24 h at 80 °C (200 rpm). The **P1**–**6@TEPA** particles were washed three times with H_2O and EtOH, each and dried at 65 °C for 16 h.

5 g of **P1**–**6@TEPA** particles were dispersed in 270 mL of 2-propanol and 30 mL of H_2O. Then 12.5 mL of TEOS and 1.25 mL of an ammonia solution were added and stirred at room temperature (130 rpm) for 24 h. The particles were separated from the solution, washed three times with H_2O and EtOH, each and dried at 65 °C for 16 h. After calcination at 600 °C for 10 h mesoporous silica microspheres **MPSM1**–**6** remained.

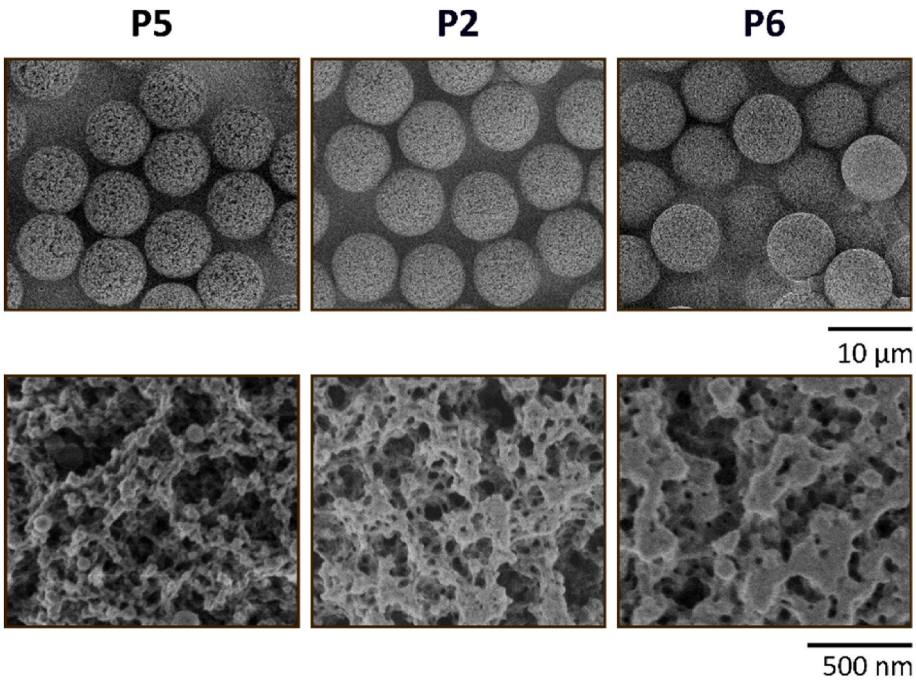

Fig. 2. SEM-images of *p*(GMA-*co*-EDMA) templates **P5**, **P2** and **P6** with increasing monomer to porogen ratio (from left to right). 2,000 (top row) and 50,000 (bottom row) magnification.

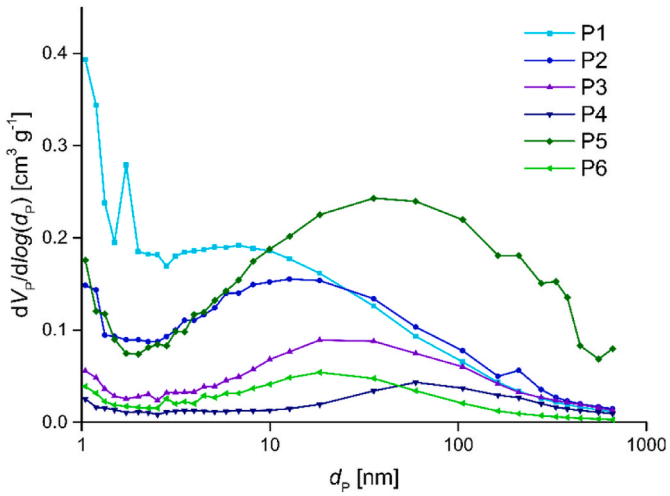

Fig. 3. Pore size distributions from the adsorption isotherms of the *p*(GMA-*co*-EDMA) templates **P1–6**.

2.3.3. *Octadecyl functionalization of **MPSM1–4** for chromatographic measurements*

5 g of **MPSM1–4** were dispersed in 600 mL of hydrochloric acid (3.7%) and stirred for 3 h at 100 °C (130 rpm). The particles were separated from the solution, washed with EtOH and H_2O until neutral and dried at 65 °C for 16 h. The particles were then dispersed in 75 mL of toluene, 25 mL of trimethoxy (octadecyl) silane (ODTMS) and 0.5 mL of triethylamine were added, and the mixture was stirred at 100 °C (130 rpm) for 6 h. The particles were separated from the solution, washed three times with toluene, three times with EtOH and twice with MeOH and dried at 65 °C for 16 h.

The functionalized particles were packed in a slurry with acetone and MeOH/H_2O (85/15 v./v.) as pressure medium.

3. Results and discussion

3.1. *Modification of p(GMA-co-EDMA) microspheres with different GMA and EDMA ratios*

The spherical porous *p*(GMA-*co*-EDMA) polymer particles **P1–6** were prepared by a seeded swelling suspension polymerization of monodisperse polystyrene (PS) microspheres [24]. PS with a diameter of 1.9 ± 0.1 µm (Fig S1, S.I.) were applied as seeds in the polymerization of glycidyl methacrylate and ethylene glycol dimethacrylate as crosslinker as well as toluene and cyclohexanol as porogens. The amount of GMA and EDMA (v./v.) and the ratio of monomers to porogens (v./v.) were varied according to Table 1.

The size and morphology of the *p*(GMA-*co*-EDMA) templates were characterized with scanning electron microscopy (SEM) (Figs. 1 and 2). The particle sizes of **P1–4** slightly decrease from 7.9 to 7.3 µm which correlates with the increasing amount of GMA (Table 1). As the density of GMA is lower than that of EDMA the swelling factor is reduced when the amount of GMA is increased at the expense of EDMA [33]. Changing the proportion of monomers to porogens at a constant GMA/EDMA ratio, increases the particle size of the template with increasing monomer content (**P5** < **P2** < **P6**, Table 1). This is attributed to the increased number of swelling monomers. All templates show a smooth morphology with different porous networks. Independent of the ratio of GMA to EDMA and the ratio of monomer to porogen uniform porous polymer templates with a narrow size distribution are obtained (Table 1, Figs. 1 and 2).

Specific surface areas, pore sizes and pore volumes of **P1–6** were determined from nitrogen adsorption isotherms (Fig. 3 and Fig S2, S.I.). All *p*(GMA-*co*-EDMA) templates (**P1–6**) display a broad pore size distribution between 5 and 100 nm (Fig. 3). In addition, contrary to the rest of the templates, **P1** shows a proportion of small pores (2 nm). With increasing amounts of monomer GMA the median pore size increases from 6 to 35 nm. Consequently, the surface areas of the particles decrease from 270 $m^2\ g^{-1}$ to 15 $m^2\ g^{-1}$ in the same order (**P1** > **P2** > **P3** > **P4**, Table 1).

The more GMA is applied the less EDMA is present, which leads to fewer branches and thus a lower degree of cross-linkage. As a result, the

pores become larger. On the other hand, a higher amount of GMA leads to earlier phase separation, which also results in larger pores [31]. The finer network structure, resulting from a higher cross-linking degree with higher EDMA ratios is also visible in the morphology of the polymer particles (Fig. 1). With increasing GMA content from **P1** to **P4**, the surface texture becomes rougher. The pore volume of the particles decreases with higher amount of GMA. Comparing the templates **P5**, **P2** and **P6** the pore parameters decrease with higher amount of monomer and consequently lesser amount of porogen. Since during the polymerization a lower proportion of porogens is present, this results in smaller pores and a smaller pore volume.

3.2. Spectral analysis of p(GMA-co-EDMA) and P@TEPA microspheres

The functionalization of the *p*(GMA-*co*-EDMA) polymer particles with amino groups provides a positive surface charge which supports the deposition of negatively charged silica species into the polymer network under sol-gel conditions [25,34]. To introduce amino functions, the porous templates **P1**–**6** were treated with tetraethylene pentamine to generate **P1**–**6@TEPA** particles via ring opening reactions of the epoxy groups (Scheme 1). As the degree of amination at the polymer surface depends on the amount of GMA incorporated into the template the number of TEPA groups and, thus, the positive charges differ in the **P1**–**6@TEPA** particles. Unfortunately, the amount of TEPA in the **P1**–**6@TEPA** particles is rather small compared to their bulk compositions, so that any changes of nitrogen content falls below the limit of detection via elemental analyses (Table S1, S.I.).

Thus, a partial least squares regression (PLS-R) model, based on FTIR spectra of the particles, which predicts the decrease in the GMA ratio through amination of polymers **P1**–**6** was applied as indirect and indicative measure. The aim is to assess differences in degrees of amination for the **P1**–**6@TEPA** particles in dependence of the initial relative GMA content.

The intensities of characteristic IR frequencies which vary with the amount of GMA are those of the symmetric and asymmetric ring vibration of the epoxide at 845 and 910 cm^{-1}, respectively [35]. The *C*–O stretching vibration of the epoxide ring at 1270 cm^{-1} also responds to changes in GMA ratio (Fig S4d, S.I.). The established PLS-R model, based on four regression coefficients, has a high predictive power with an $R^2_{pred} = 0.9922$ and a low error with RMSEP = 0.6% and can hence be used to effectively determine the relative ratio of GMA in **P1**–**6@TEPA** (Fig S4a-c, S.I.).

After the functionalization with TEPA, the vibrations corresponding to the epoxide groups decrease in absorbance. Consequently, the intensities of the vibrations from the epoxy groups decrease within increasing functionalization of the particles (Fig. 4a). The established PLS-R was used for the prediction of the GMA content of **P1**–**6** and **P1**–**6@TEPA** particles. The predicted values are given in Fig. 4b. The low deviations of predicted values from the actual values of the polymers and the small standard deviation for each prediction indicate a high model accuracy (Table 2, Fig. 4b).

The predicted residual GMA ratios for the amino functionalized particles **P1@TEPA** to **P6@TEPA**, respectively, correspond to a decrease in epoxy ratio during amination, respectively (Table 2). The degree of TEPA functionalization follows the order **P1** < **P5** ~ **P6** < **P2** < **P3** < **P4**.

3.3. Preparation of mesoporous silica microspheres (MPSM1–6)

The **P1**–**6@TEPA** particles were applied as hard templates in a base catalyzed sol-gel process. In the presence of 2-propanol and H_2O, the corresponding amino functionalized polymer templates, and tetraethyl orthosilicate (TEOS) formed polymer/silica hybrid beads (**HB1**–**6,** Scheme 1, and Figs. S5 and S6 and Table S2, S.I.). Calcination of the **HB1**–**6** at 600 °C for 10 h removed the organic polymer which leaves the mesoporous silica particles **MPSM1**–**6** (Scheme 1 and Figs. 5 and 6) (see

Table 2
Actual and predicted GMA ratios of **P1**–**6** and **P1**–**6@TEPA**.

	actual GMA ratio of *p* (GMA-*co*-EDMA)	predicted GMA ratio		predicted GMA ratio of P@TEPA	Δ *p*(GMA-*co*-EDMA) – P@TEPA
P1	20	20.6	**P1@TEPA**	16.1	4.5
P2	40	38.9	**P2@TEPA**	29.4	9.5
P3	60	60.9	**P3@TEPA**	49.1	11.8
P4	80	79.6	**P4@TEPA**	65.6	14.1
P5	40	39.2	**P5@TEPA**	32.1	7.1
P6	40	39.5	**P6@TEPA**	32.6	6.9

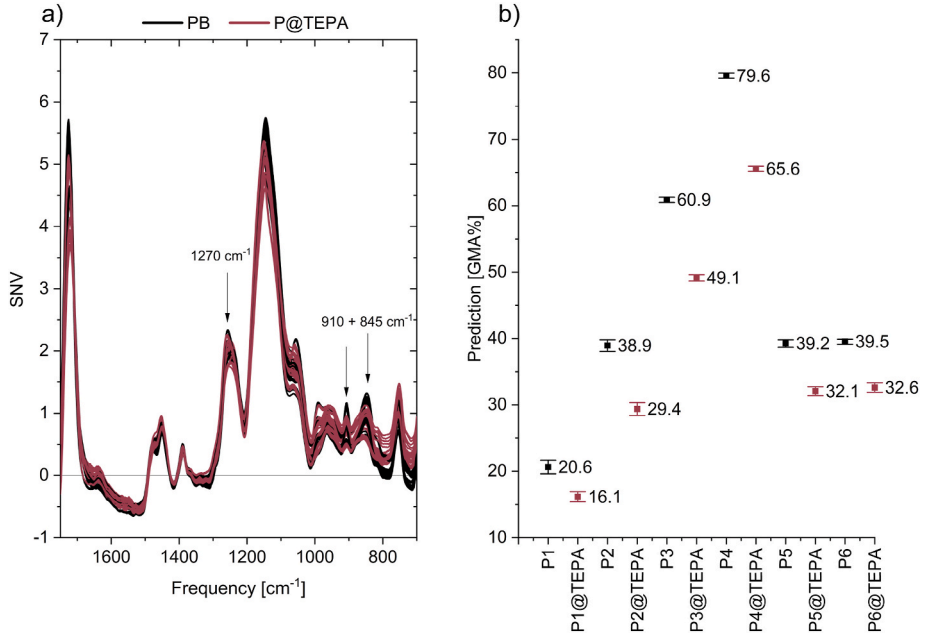

Fig. 4. a) Spectra of **P1–6** and **P1–6@TEPA** templates after spectral preprocessing with standard normal variate transformation and b) predicted values of mean epoxy content with standard deviation across all spectra used for prediction. **P1–6** are depicted in black and **P1–6@TEPA** templates in red.

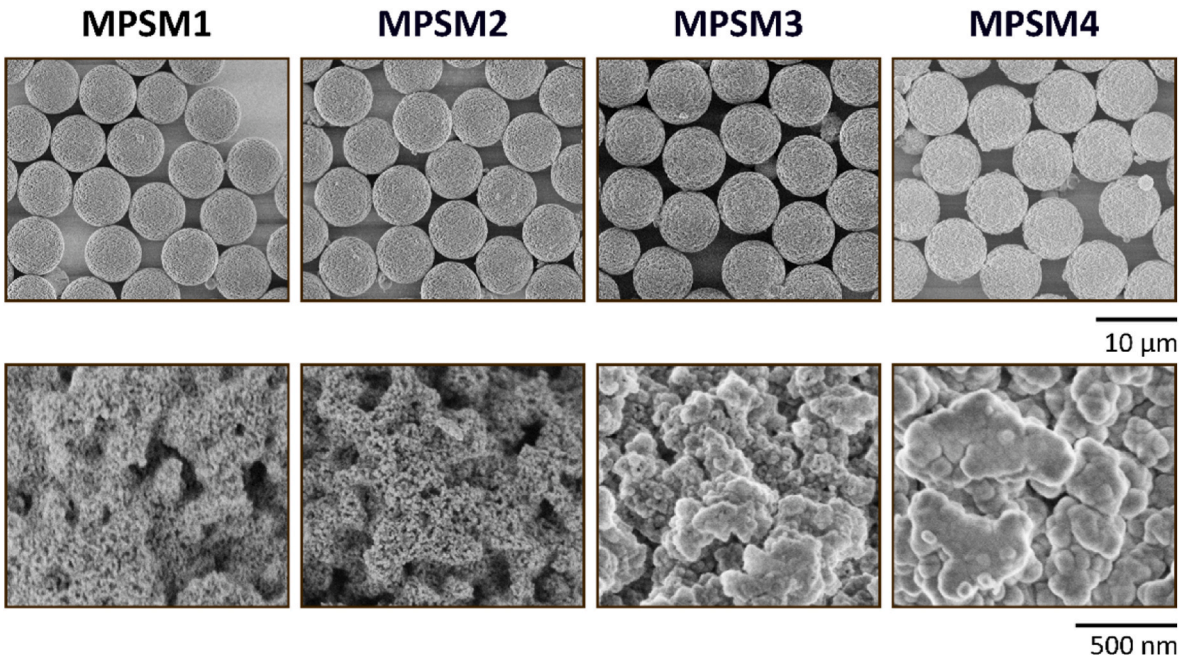

Fig. 5. SEM images of mesoporous silica microspheres **MPSM1**–**4** using polymer templates with different amount of GMA. 2,000 (top row) and 50,000 (bottom row) magnification.

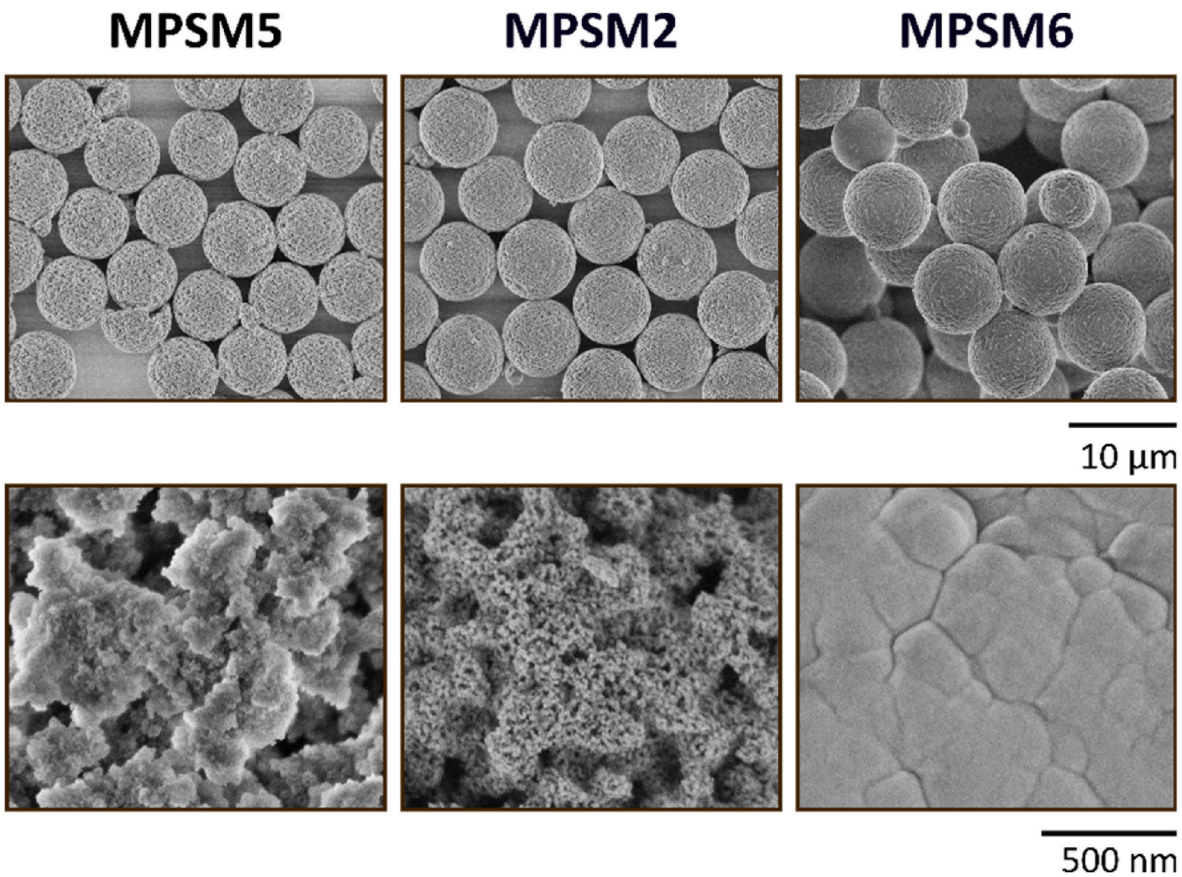

Fig. 6. SEM images of mesoporous silica microspheres **MPSM2,5,6** using polymer templates with different monomer to porogen ratio. 2,000 (top row) and 50,000 (bottom row) magnification.

Fig. 7).

An evaluation of the SEM images of **MPSM1**–**6** show that the high monodispersity as specified by the template particles is maintained (Figs. 5 and 6, Tables 1 and 3). Although the diameters of the templates **P1**–**6@TEPA** differ by only 0.6 µm (Table 1), the range of silica particle size is extended to 1.6 µm (Table 3). The smallest silica particles **MPSM1**

Table 3
Properties of mesoporous silica microspheres **MPSM1–6**.

	particle size	dispersity	median pore size	pore volume	specific surface area
	[µm]	d_{90}/d_{10}	[nm][a]	[$cm^3\ g^{-1}$]	[$m^2\ g^{-1}$]
MPSM1	6.6	1.2	15.4	0.71	342
MPSM2	6.8	1.2	19.2	0.56	252
MPSM3	7.0	1.2	23.0	0.22	139
MPSM4	7.1	1.2	72.4	0.12	68
MPSM5	6.3	1.1	12.1	0.88	382
MPSM6	8.2	1.1	–	–	–

[a] From desorption isotherms.

and **MPSM5** with a particle size of 6.3 and 6.6 µm, respectively, result from those templates which contain the smallest amount of TEPA (**P1@TEPA** and **P5@TEPA**). With increasing amount of TEPA in the templates (Table 2) the silica materials become larger (**MPSM2**, **MPSM3** and **MPSM4**). Interestingly, **MPSM6** with a particle size of 8.2 µm is larger than the corresponding **P6@TEPA** template (Tables 1 and 3). In this case also non-porous secondary nanoparticles with a size of 230 nm were found in the filtrate of the washing procedure (Fig S7, S.I.). The morphology of **HB6** and **MPSM6** (Fig S5 and Fig. 6) indicate that the pores of the template are closed, and large silica nanoparticles aggregate to a shell around the template. SEM images of purposely destroyed **MPSM6** show that the particles are hollow and a shell of silica remains after calcination (Fig S8, S.I.) The silica network of **MPSM1** and **MPSM2** is made up of small nanometer-sized silica particles which create many small pores and a rough surface (Fig. 5). With increasing amount of TEPA the SNPs become larger (**MSMP3** and **MSMP4**), the number of small particles is declining and the surface becomes smoother (Fig. 5).

Removing the organic template leaves more space behind so that the median pore sizes, pore volumes and specific surface areas of **MPSM1**–**5** increase compared to those of the corresponding polymer particles **P1**–**5** (Table 2). Moreover, the pore parameters of **MPSMs** follow the same course as those of the polymer particles. Based on the t-plots of the adsorption isotherms, the MPSMs do not exhibit microporosity and possess pre-dominantly mesopores.

The mesoporous silica microspheres **MPSM1**–**6** are composed of non-porous silica nanoparticles of different size and shape. The size of the SNPs and their deposition into the template depends on three factors: (i) the rate of the growth of the SNPs in the continuous phase which is based on the sol-gel parameters, (ii) the diffusion rate of the SNPs into the template which is controlled by the ability of the template to attract negatively charged SNPs from the solution and (iii) the pore parameters of the template. For all experiments the sol-gel process parameters are the same and thus the rates of the SNP growth are comparable. This agrees with the overall amount of deposited silica (30 wt%) into the porous polymer network independent of the polymer composition (Fig. S9, S.I.).

Under the present reaction conditions the amino groups of the attached TEPA functions are still partly protonated which provides the template surface with a positive charge. A higher amount of TEPA generates a higher positive charge. Templates with higher TEPA content extract negatively charged silica species from the reaction mixture at an early state of the SNP growth. Small silica particles are deposited in the pores of the template where they aggregate and form larger SNPs. This is the case for **MPSM4** and **6**. Furthermore, the larger pore structure of the **P4@TEPA** template provides more space for agglomeration resulting in larger SNPs. In case of **P6@TEPA** the combination of small pores and large SNPs closed the pores at the surface of the template. A silica shell around the polymer is observed. At a lower TEPA content, the attraction of SNPs is weaker, so that they diffuse into the template at a later state of the growth process. Consequently, the SNPs are larger when they are incorporated into the silica network and maintain their size as they are more stable than the smaller SNPs. In the case of **MPSM1**, a particle size of the SNPs of about 15 nm is observed.

*3.4. Protein separation using C_{18}-functionalized **MPSM1–4** as stationary phases*

Functionalization of silica materials to generate reverse stationary phases with trimethoxy (octadecyl) silane is an established method that is widely used [36]. Thus the **MPSM1-4** with different pore parameters were functionalized with trimethoxy (octadecyl) silane (C_{18}) and packed into 250 × 4.6 mm stainless steel columns using the slurry method. **MPSM5** and **MPSM6** were too fragile and broke during the packing process. The resulting reversed phase columns **MPSM1-C_{18}**-**MPSM4-C_{18}**, and the commercially available column ProSphere C18, (300 Å, 10 µm, 250 × 4.6 mm) as reference, were applied for the separation of a protein mixture consisting of ribonuclease A, cytochrome C, holo-transferrin and apomyoglobin. The chromatograms in Fig. 8 show a baseline separation of the proteins with all prepared C_{18} columns. Thus, the prepared packing materials show a separation efficiency comparable to those of the commercial column. Also, the resolutions (Table 4) between the protein peaks are comparable or even better than that of the commercially available column. Overall, the separation efficiency increases from **MPSM1-C_{18}** to **MPSM3-C_{18}**. This correlates well with the increase in median pore size of the **MPSM** packing material, as the accessibility for bigger proteins is facilitated. Especially the resolution between cytochrome C and holo-transferrin ($R_{2\text{-}3}$, Table 4) increase with increasing GMA ratio in the polymeric template which corresponds well to the increased pore sizes of **MPSM3**. Also, the overall peak symmetry is improved. For **MPSM4** the larger SNPs at the surface and the nearly closed morphology restrict the diffusion into the pores, resulting in broader peaks and decreasing column performance.

4. Conclusion

Non-porous SNPs are the building blocks of the mesoporous silica microspheres (**MPSM1-6**) prepared by the hard template assisted approach. Both pore properties and degree of amino-functionalization of the templates have a strong impact on the size of the deposited SNPs. A low proportion of GMA with small pores (**P1**) and large pores (**P5**) leads to small inserted SNPs. A high proportion of GMA with small pores (**P6**) results in the formation of a hollow silica shell. If the pores are large enough as in **P4** large SNPs can be incorporated. Thus the particle and pore properties of the **MPSM1-6** are controlled by the size of the SNPs. Small nanoparticles generate small pore sizes and high specific surface

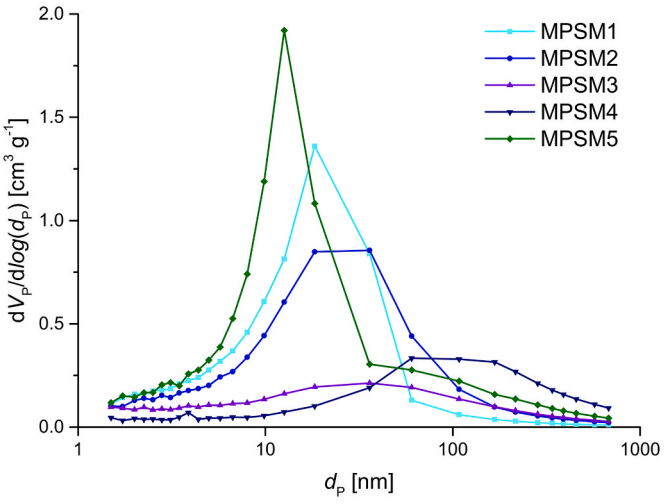

Fig. 7. Pore size distributions from the desorption isotherms of the mesoporous silica microspheres **MPSM1–5**.

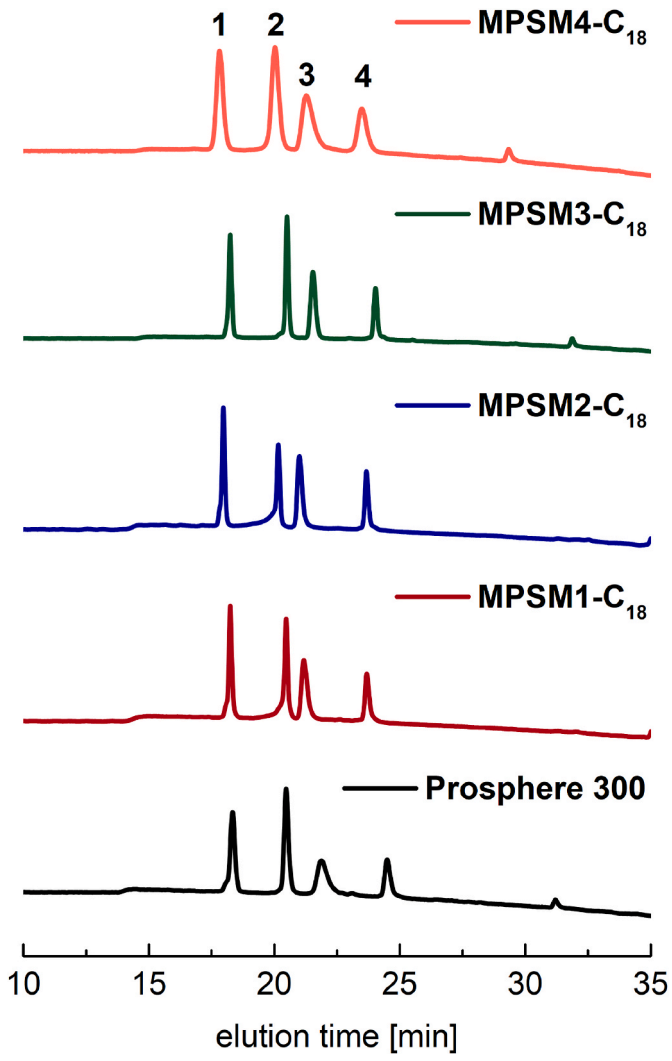

Fig. 8. Chromatograms of protein mixture H2899 separation with the prepared C_{18} functionalized stationary phases and a commercially available ProSphere 300. Chromatographic settings: column dimension: 250 × 4.6 mm; mobile phase A: H_2O with 0.1% TFA, mobile phase B: ACN with 0.08% TFA; gradient from 20% B to 85% B within 25 min; test mixture: 4 mg mL^{-1} (each 1 mg mL^{-1}) with 5 μL injection volume, 1 – ribonuclease A, 2 – cytochrome C, 3 – holo-transferrin, 4 – apomyoglobin; column temperature: 30 °C; detection wavelength: 215 nm.

Table 4
Column performance for separation of protein mixture H2899 of the **MPSM-C_{18}** columns and a commercially available column.

	Resolution R_{1-2}	Resolution R_{2-3}	Resolution R_{3-4}
MPSM1-C_{18}	9.39	1.97	6.56
MPSM2-C_{18}	9.39	2.67	8.20
MPSM3-C_{18}	9.74	3.37	7.63
MPSM4-C_{18}	4.10	1.74	2.88
ProSphere 300	6.24	2.49	4.36

areas, while larger nanoparticles lead to larger pores and lower surface areas of **MPSMs**. Interestingly, the GMA to EDMA ratio and the monomer to porogen ratio in the preparation of the template control the pore parameters of the final **MPSMs**. This allows access to stationary phases for specific separation problems in HPLC.

CRediT authorship contribution statement

Fabio Fait: Writing – original draft, Visualization, Methodology, Investigation, Data curation. **Julia C. Steinbach:** Visualization, Methodology, Investigation, Formal analysis, Data curation, Writing – original draft. **Andreas Kandelbauer:** Writing – review & editing, Supervision, Project administration, Funding acquisition, Conceptualization. **Hermann A. Mayer:** Writing – review & editing, Supervision, Resources, Project administration, Funding acquisition, Data curation, Conceptualization.

Declaration of competing interest

The authors declare that they have no known competing financial interests or personal relationships that could have appeared to influence the work reported in this paper.

Data availability

Data will be made available on request.

Acknowledgments

This research was funded the by Bundesministerium für Bildung und Forschung (BMBF, grant number 13FH647IX6) and the Bundesministerium für Wirtschaft und Energie (AiF/ZIM, grant number ZF4019203SL8). Furthermore, we would like to thank our cooperation partner Dr. Maisch GmbH for their support in preparing the columns. We thank Elke Nadler for contributing the SEM measurements.

Appendix A. Supplementary data

Supplementary data to this article can be found online at https://doi.org/10.1016/j.micromeso.2023.112482.

References

[1] G.P. Bierwagen, Sol–gel coatings on metals for corrosion protection, Prog. Org. Coating 64 (2009) 327–338.
[2] J.J. Chruściel, E. Leśniak, Modification of epoxy resins with functional silanes, polysiloxanes, silsesquioxanes, silica and silicates, Prog. Polym. Sci. 41 (2015) 67–121.
[3] C.M. Crudden, M. Sateesh, R. Lewis, Mercaptopropyl-Modified mesoporous silica: a remarkable support for the preparation of a reusable, heterogeneous palladium catalyst for coupling reactions,, J. Am. Chem. Soc. 127 (2005) 10045–10050.
[4] J. Wei, Z. Sun, W. Luo, Y. Li, A.A. Elzatahry, A.M. Al-Enizi, Y. Deng, D. Zhao, New insight into the synthesis of large-pore ordered mesoporous materials, J. Am. Chem. Soc. 139 (2017) 1706–1713.
[5] K.W. Gallis, J.T. Araujo, K.J. Duff, J.G. Moore, C.C. Landry, The use of mesoporous silica in liquid chromatography, Adv. Mater. 11 (1999) 1452–1455.
[6] B.M. Wagner, S.A. Schuster, B.E. Boyes, J.J. Kirkland, Superficially porous silica particles with wide pores for biomacromolecular separations, J. Chromatogr. A 1264 (2012) 22–30.
[7] J.J. Kirkland, F.A. Truszkowski, C.H. Dilks, G.S. Engel, Superficially porous silica microspheres for fast high-performance liquid chromatography of macromolecules, J. Chromatogr. A 890 (2000) 3–13.
[8] L.F. Giraldo, B.L. López, L. Pérez, S. Urrego, L. Sierra, M. Mesa, Mesoporous silica applications, Macromol. Symp. 258 (2007) 129–141.
[9] M. Ide, E. Wallaert, I. Van Driessche, F. Lynen, P. Sandra, P. Van Der Voort, Spherical mesoporous silica particles by spray drying: doubling the retention factor of HPLC columns, Microporous Mesoporous Mater. 142 (2011) 282–291.
[10] K.K. Unger, R. Skudas, M.M. Schulte, Particle packed columns and monolithic columns in high-performance liquid chromatography-comparison and critical appraisal, J. Chromatogr. A 1184 (2008) 393–415.
[11] R. Hayes, A. Ahmed, T. Edge, H. Zhang, Core–shell particles: preparation, fundamentals and applications in high performance liquid chromatography, J. Chromatogr. A 1357 (2014) 36–52.
[12] M.C. Kimling, R.A. Caruso, Sol–gel synthesis of hierarchically porous TiO2 beads using calcium alginate beads as sacrificial templates, J. Mater. Chem. 22 (2012) 4073.
[13] W. Liu, C. Selomulya, W. Wu, X.D. Chen, A single step assembly of uniform microparticles for controlled release applications,, Soft Matter 7 (2011) 3323.
[14] I.V. Melnyk, B. Alonso, Y.L. Zub, E. Véron, D. Massiot, T. Cacciaguerra, Spray-dried mesoporous silica microspheres with adjustable textures and pore surfaces

homogenously covered by accessible thiol functions, J. Mater. Chem. 18 (2008) 1368.
[15] K. Waldron, Z. Wu, W.D. Wu, W. Liu, D. Zhao, X.D. Chen, C. Selomulya, Formation of uniform large SBA-15 microspheres via spray drying, J. Mater. Chem. 2 (2014) 19500–19508.
[16] W. Stöber, A. Fink, E. Bohn, Controlled growth of monodisperse silica spheres in the micron size range, J. Colloid Interface Sci. 26 (1968) 62–69.
[17] N. Plumeré, A. Ruff, B. Speiser, V. Feldmann, H.A. Mayer, Stöber silica particles as basis for redox modifications: particle shape, size, polydispersity, and porosity, J. Colloid Interface Sci. 368 (2012) 208–219.
[18] S.-L. Chen, P. Dong, G.-H. Yang, J.-J. Yang, Characteristic aspects of formation of new particles during the growth of monosize silica seeds, J. Colloid Interface Sci. 180 (1996) 237–241.
[19] K. Nozawa, H. Gailhanou, L. Raison, P. Panizza, H. Ushiki, E. Sellier, J.P. Delville, M.H. Delville, Smart control of monodisperse stöber silica Particles: effect of reactant addition rate on growth process, Langmuir 21 (2005) 1516–1523.
[20] H. Nakabayashi, A. Yamada, M. Noba, Y. Kobayashi, M. Konno, D. Nagao, Electrolyte-added one-pot synthesis for producing monodisperse, micrometer-sized silica particles up to 7 μm, Langmuir 26 (2010) 7512–7515.
[21] C.T. Kresge, M.E. Leonowicz, W.J. Roth, J.C. Vartuli, J.S. Beck, Ordered mesoporous molecular sieves synthesized by a liquid-crystal template mechanism, Nature 359 (1992) 710–712.
[22] N.K. Raman, M.T. Anderson, C.J. Brinker, Template-based approaches to the preparation of amorphous, nanoporous silicas, Chem. Mater. 8 (1996) 20.
[23] L. Zhang, L. Jin, B. Liu, J. He, Templated growth of crystalline mesoporous materials: from soft/hard templates to colloidal templates, Front. Chem. 7 (2019) 22.
[24] H. Xia, G. Wan, J. Zhao, J. Liu, Q. Bai, Preparation and characterization of monodisperse large-porous silica microspheres as the matrix for protein separation, J. Chromatogr. A 1471 (2016) 138–144.
[25] J. Chen, L. Zhu, L. Ren, C. Teng, Y. Wang, B. Jiang, J. He, Fabrication of monodisperse porous silica microspheres with a tunable particle size and pore size for protein separation, ACS Appl. Bio Mater. 1 (2018) 604–612.
[26] J. Bai, Q. Zhu, C. Tang, J. Liu, Y. Yi, Q. Bai, Synthesis and application of 5 μm monodisperse porous silica microspheres with controllable pore size using polymeric microspheres as templates for the separation of small solutes and proteins by high-performance liquid chromatography, J. Chromatogr. A 1675 (2022) 463165.
[27] V. Šmigol, F. Švec, Synthesis and properties of uniform beads based on macroporous copolymer glycidyl methacrylate–ethylene dimethacrylate: a way to improve separation media for HPLC,, J. Appl. Polym. Sci. 46 (1992) 1439–1448.
[28] S. Grama, D. Horák, Preparation of monodisperse porous silica particles using poly (glycidyl methacrylate) microspheres as a template, Physiol. Res. (2015) 11–17.
[29] L.C. Costa, R.C. Monteiro, H.M.A. Castro, T.S. Ribeiro, M.A. Oliveira, E.C. C. Torquato, M.E. Arcanjo, M.R.C. Marques, Glycidyl methacrylate-ethylene glycol dimethacrylate copolymers with varied pore structures prepared with different reaction parameters, Mat. Res. 23 (2020), e20190550.
[30] J. He, C. Yang, X. Xiong, B. Jiang, Preparation and characterization of monodisperse porous silica microspheres with controllable morphology and structure, J. Polym. Sci. Polym. Chem. 50 (2012) 2889–2897.
[31] J.C. Steinbach, F. Fait, S. Wagner, A. Wagner, M. Brecht, H.A. Mayer, A. Kandelbauer, Rational design of pore parameters in monodisperse porous poly (glycidyl methacrylate-co-ethylene glycol dimethacrylate) particles based on response surface methodology, Polymers 14 (2022) 382.
[32] J.C. Groen, L.A.A. Peffer, J. Pérez-Ramírez, Pore size determination in modified micro- and mesoporous materials. Pitfalls and limitations in gas adsorption data analysis, Microporous Mesoporous Mater. 60 (2003) 1–17.
[33] K. Hosoya, J.M.J. Fréchet, Influence of the seed polymer on the chromatographic properties of size monodisperse polymeric separation media prepared by a multi-step swelling and polymerization method, J. Polym. Sci. Polym. Chem. 31 (1993) 2129–2141.
[34] J.C. Steinbach, F. Fait, H.A. Mayer, A. Kandelbauer, Monodisperse porous silica/polymer nanocomposite microspheres with tunable silica loading, morphology and porosity, Int. J. Mol. Sci. 23 (2022) 14977.
[35] G. Socrates, Infrared and Raman Characteristic Group Frequencies: Tables and Charts, third ed., John Wiley & Sons Inc, 2004.
[36] H.A. Claessens, M.A. van Straten, Review on the chemical and thermal stability of stationary phases for reversed-phase liquid chromatography, J. Chromatogr. A 1060 (2004) 23–41.